Stem Cell Reports
Article

ISSCR

OPEN ACCESS

Directed Differentiation of Human Bone Marrow Stromal Cells to Fate-Committed Schwann Cells

Sa Cai,[1] Yat-Ping Tsui,[1] Kin-Wai Tam,[1] Graham Ka-Hon Shea,[2] Richard Shek-Kwan Chang,[3] Qiang Ao,[5] Daisy Kwok-Yan Shum,[1,4,*] and Ying-Shing Chan[1,4,*]

[1]School of Biomedical Sciences, Li Ka Shing Faculty of Medicine
[2]Department of Orthopaedics & Traumatology, Li Ka Shing Faculty of Medicine
[3]Department of Medicine, Li Ka Shing Faculty of Medicine
[4]State Key Laboratory of Brain and Cognitive Science
The University of Hong Kong, Hong Kong, Hong Kong SAR
[5]Department of Tissue Engineering, China Medical University, Shenyang, PR China
*Correspondence: shumdkhk@hku.hk (D.K.-Y.S.), yschan@hku.hk (Y.-S.C.)
http://dx.doi.org/10.1016/j.stemcr.2017.08.004

SUMMARY

Our ultimate goal of *in vitro* derivation of Schwann cells (SCs) from adult bone marrow stromal cells (BMSCs) is such that they may be used autologously to assist post-traumatic nerve regeneration. Existing protocols for derivation of SC-like cells from BMSCs fall short in the stability of the acquired phenotype and the functional capacity to myelinate axons. Our experiments indicated that neuro-ectodermal progenitor cells among the human hBMSCs could be selectively expanded and then induced to differentiate into SC-like cells. Co-culture of the SC-like cells with embryonic dorsal root ganglion neurons facilitated contact-mediated signaling that accomplished the switch to fate-committed SCs. Microarray analysis and *in vitro* myelination provided evidence that the human BMSC-derived SCs were functionally mature. This was reinforced by repair and myelination phenotypes observable *in vivo* with the derived SCs seeded into a nerve guide as an implant across a critical gap in a rat model of sciatic nerve injury.

INTRODUCTION

Although Schwann cells (SCs) have a major role as the myelin-forming glial cells of the peripheral nervous system (PNS), they switch on an axon-supportive program in response to nerve injury. The injury-triggered reprogramming engages SCs in myelin breakdown (Gomez-Sanchez et al., 2015; Martini et al., 2008), neurotrophic factor production (Brushart et al., 2013), guidance of axonal regrowth (Rosenberg et al., 2014), and eventually axonal re-myelination (Chen et al., 2007). This repair mode of SCs is not shared by the CNS counterpart, oligodendrocytes (Brosius Lutz and Barres, 2014). The SCs have therefore been tapped to assist post-traumatic nerve regeneration in the PNS (Rodriguez et al., 2000) and CNS (Bachelin et al., 2005). To take advantage of the unique plasticity of SCs, however, sufficient numbers of SCs are required, ideally without having to sacrifice a peripheral nerve for the graft.

This need is in part addressed by *in vitro* derivation of SC-like cells (SCLCs) from bone marrow stromal cells (BMSCs) with a cocktail of glia-inducing factors (GIFs) (Caddick et al., 2006; Dezawa et al., 2001; Keilhoff et al., 2006). The derived SCLCs however tended to be phenotypically unstable and demonstrated limited capacity for re-myelination. This issue was overcome in an *in vitro* course by which the SCLCs acquired competence and commitment to the SC fate (Shea et al., 2010). Thereafter, the derived SCs demonstrated capability to myelinate regrowing axons not only *in vitro* but also *in vivo* (Ao et al., 2011).

Here, in anticipation of clinical application of BMSC-derived SCs, we take a leap from the rat protocol to a human protocol. Starting from human BMSCs (hBMSCs) expressing mesenchymal markers CD44, CD90, and CD105, we propagated spheres with constituent cells expressing the neuroglial progenitor markers, nestin and glial fibrillary acidic protein (GFAP). With sphere cells in adherent culture and soluble supplements in the medium, cells progressively assumed the bi-/tri-polar morphology of SCLCs and expressed such markers as p75NTR and S100. Co-culture of the hBMSC-derived SCLCs with rat dorsal root ganglion (DRG) neurons provided proof of principle that juxtacrine signaling between the neurons and SCLCs in co-culture accomplishes *in vitro* commitment of SCLCs to the SC fate. Like the rat counterpart, hBMSC-derived SCs demonstrated myelinating capacity both *in vitro* and *in vivo*.

RESULTS

Characterization of hBMSCs

Primary hBMSCs adherent on tissue-culture plastic showed the characteristically flattened, fibroblastic-like morphology (Figure S1A). The hBMSCs were positive for the mesenchymal markers, CD73, CD90, and CD105 (immunofluorescence; Figures S1B–S1D) at 94.6%, 92.0%, and 76.4%, respectively (flow cytometry; Figures S1E–S1G). Following adherent culture of the hBMSCs, 8.1% ± 2.2% (n = 6) were nestin positive (Figures 1Aa and 1Ag) and none were GFAP

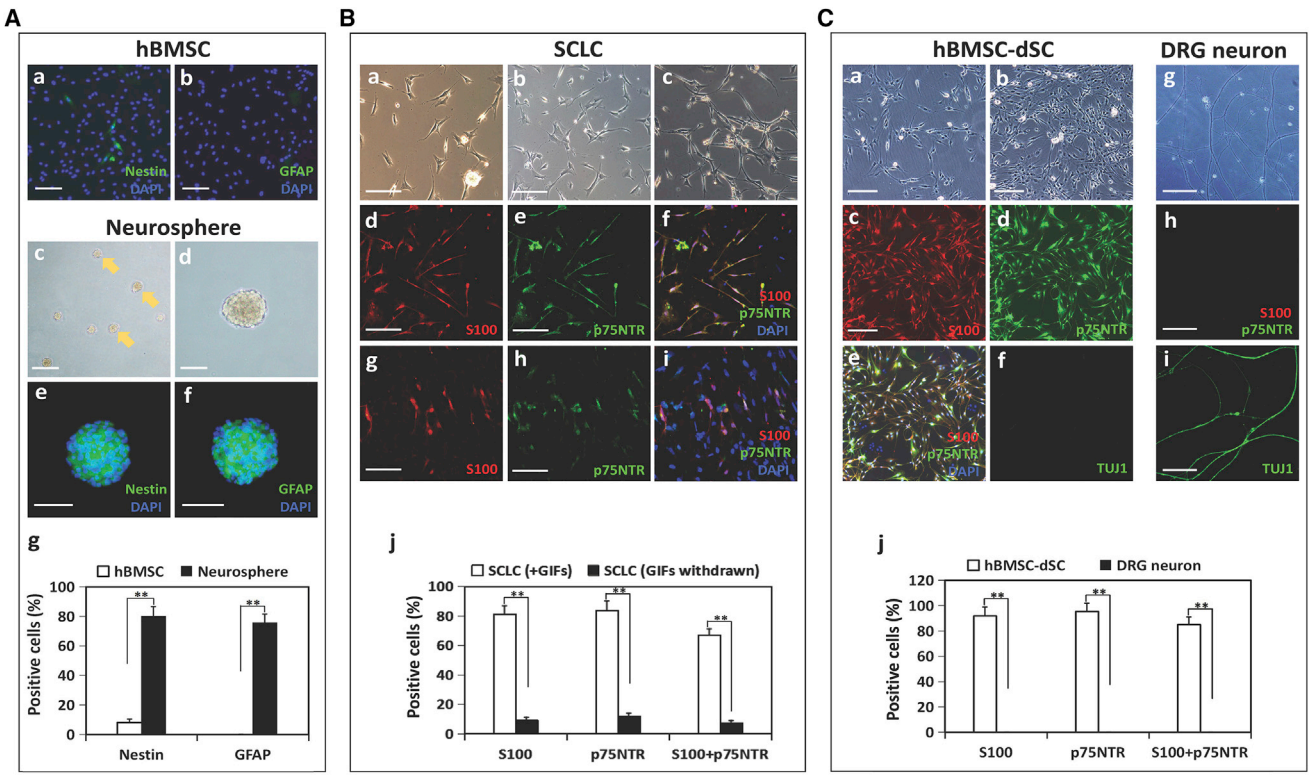

Figure 1. Directed Differentiation of hBMSCs to Fate-Committed SCs

(A) Neurospheres derived from hBMSCs. (a, b) Representative images of hBMSCs in adherent culture as viewed under epifluorescence microscopy, being largely immunonegative for nestin and GFAP. (c) Representative image of spheres (arrowheads) on day 10 following transfer of hBMSCs to non-adherent culture in sphere-forming medium. (d, e, f) Representative images of spheres continuing to day 14 in non-adherent, sphere-forming culture. At this stage, the neurosphere cells become largely immunopositive for nestin and GFAP (e, f, and g), in contrast to the hBMSCs (g). **p < 0.01, hBMSC-derived neurosphere versus hBMSC. Scale bar, 100 μm. n = 6 independent experiments.

(B) Differentiation of hBMSC-derived neurospheres into SCLCs. Phase-contrast images showing cells exiting from neurospheres on day 3 (a) and day 5 (b) of adherent culture in α-MEM supplemented with GIFs and gradually assuming bi- and tri-polar morphologies typical of SCs in culture on day 7 (c). Immunofluorescence for S100 and p75NTR among neurosphere-derived SCLCs in α-MEM supplemented with GIFs (+GIFs) (d, e, merged in f) contrasting immunonegativity for the markers in DMEM/F12 with GIFs withdrawn (g, h, merged in i). Histogram showing percentages of SCLCs immunopositive for the indicated markers in cultures supplemented with GIFs (+GIFs) versus those with GIFs withdrawn (j). **p < 0.01, SCLC (+GIFs) versus SCLC (GIFs withdrawn). Scale bar, 100 μm. n = 6 independent experiments.

(C) Commitment of SCLCs to the SC fate following co-culture with DRG neurons. Phase-contrast images of hBMSC-dSCs in basal medium without GIF supplementation or DRG neurons on day 3 (a) and day 7 (b). Phase-contrast image of a parallel-culture purified DRG neurons (g). hBMSC-dSCs that are S100- and p75NTR-positive (c, d, merged in e) but TUJ1-negative (f), contrasting DRG neurons that are S100- and p75NTR-negative (h) but TUJ1-positive (i). Histogram showing percentages of hBMSC-dSCs immunopositive for the indicated markers versus null for purified DRG neurons (j). **p < 0.01, hBMSC-dSC versus DRG neuron. Scale bar, 100 μm. n = 6 independent experiments.

positive (Figures 1Ab and 1Ag), suggesting the occurrence of a neuroprogenitor subpopulation in the preparation.

Enrichment of Neuroprogenitor Cells in Sphere-Forming Culture

Under sphere-forming conditions, the hBMSCs transitioned into floating spheres, visible by day 10 (Figure 1Ac) and expandable to ≥150 μm in diameter by day 14 (Figures 1Ad and S2). The increase in proportion of cells expressing the neural stem/progenitor markers, nestin (80.2% ± 6.3% of the sphere cells, n = 6; Figures 1Ae and 1Ag) and GFAP (75.7% ± 5.7% of the sphere cells, n = 6; Figures 1Af and 1Ag) was reinforced by western blot analysis of cell lysates (Figure 2A). The results indicate successful propagation of neuroprogenitors among the hBMSCs in sphere-forming culture.

Directed Differentiation to SCLCs

Adherent culture of sphere cells in medium supplemented with GIFs fostered transition to spindle-like cells in 3 days

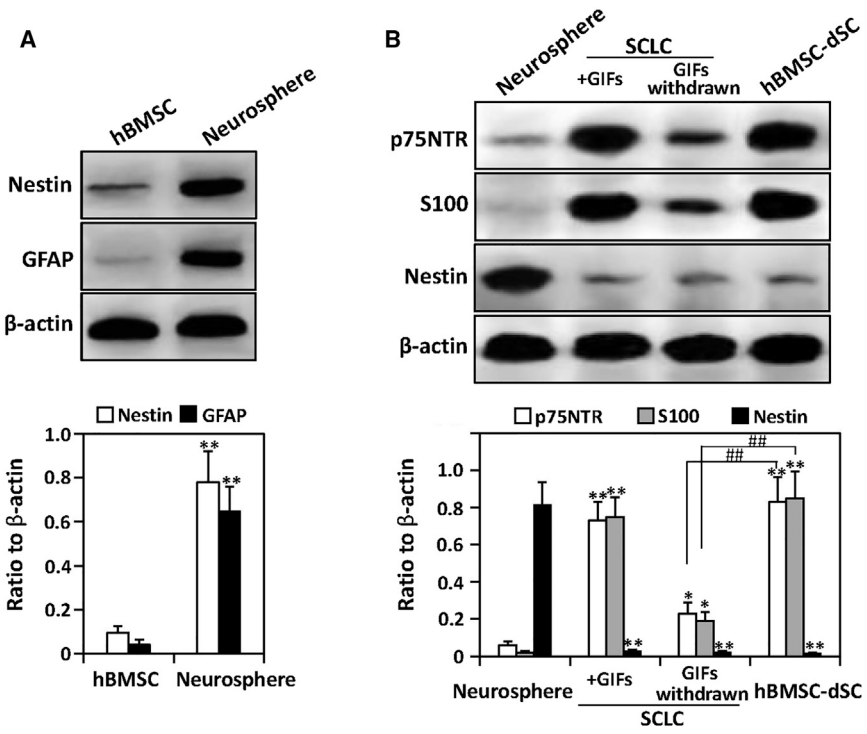

Figure 2. Marker Protein Profiles of hBMSCs, Neurosphere Cells, SCLCs, and hBMSC-dSCs

(A) Western blot analysis for nestin and GFAP in lysates of hBMSCs and hBMSC-derived neurosphere cells (upper). Plots of densitometric scans of band intensity as normalized against that of β-actin (lower). **p < 0.01, neurosphere cells versus hBMSC. n = 6 independent experiments.

(B) Western blot analysis for p75NTR, S100, and nestin in lysates of the respective hBMSC-derived cell types (neurosphere cells, SCLCs maintained in culture with GIF supplementation (+GIFs) and then 3 days after GIF withdrawal (GIFs withdrawn), and hBMSC-dSCs) (upper). Plots of densitometric scans of band intensity as normalized against that of β-actin (lower). *p < 0.05, **p < 0.01, SCLC (+GIFs) and SCLC (GIFs withdrawn) versus neurosphere cells. ##p < 0.01, hBMSC-dSC versus SCLC (GIFs withdrawn). n = 6 independent experiments.

(Figure 1Ba) and SC-like morphology with extended processes in 5–7 days (Figures 1Bb and 1Bc). At this stage, 81.3% ± 5.4% (n = 6) of the cells were positive for S100 (Figures 1Bd and 1Bj) and 83.6% ± 6.5% (n = 6) were positive for p75NTR (Figures 1Be and 1Bj); 66.9% ± 4.1% of the cells co-expressed S100 and p75NTR (Figures 1Bf and 1Bj). However, these phenotypic features were not sustainable following withdrawal of the GIFs from the cultures; in 3 days, the cells became fibroblast-like, and immunopositivities for the SC markers, S100 and p75NTR, were down to 9.2% ± 1.6% (Figures 1Bg and 1Bj) and 11.8% ± 1.9% (Figures 1Bh and 1Bj) respectively. Only 7.6% ± 1.1% of the cells co-expressed S100 and p75NTR (Figures 1Bi and 1Bj). The GIFs could therefore not specify commitment to the SC fate.

Commitment of SCLCs to SC Fate

As proof of principle that contact-mediated signaling between sensory neurons and hBMSC-derived SCLCs is necessary for transition to fate commitment, the SCLCs were seeded onto purified rat DRG neuron networks. On day 1 of co-culture, SCLCs remained fibroblast-like; from day 7, they adopted bi-/tri-polar morphology with tapering processes typical of SCs in culture (Figure S3). Neurons were detectable in proximity to the tapering SCLCs in the co-culture. In passaging the co-cultures, neurons did not survive (TUJ1 negative; Figure 1Cf), resulting in mono-cultures of SCLCs that persisted both in morphology (3 days, Figure 1Ca; 7 days, Figure 1Cb) and marker expression as revealed via immunocytochemistry (S100, 91.8% ± 7% of cells; p75NTR, 95.3% ± 6.5%; both S100 and p75NTR, 84.9% ± 6% of cells) (n = 6; Figures 1Cc, 1Cd, 1Ce, and 1Cj) and western blot analysis (Figure 2B). Control cultures of purified DRG neurons maintained in parallel showed no signs of SCs in terms of marker expression (Figures 1Cg, 1Ch, and 1Cj) and morphology (Figures S3D–S3F), whereas the TUJ1-positive neurite network was clearly detectable (Figure 1Ci). We therefore ruled out the possibility that SCs observed in the co-culture arose from contaminating glia in the DRG neuron preparation. The SCLC descendants of the co-culture, having survived GIF withdrawal and neuron removal, are therefore committed to the SC fate and named as hBMSC-derived SCs (hBMSC-dSCs).

In Vitro Myelination by hBMSC-dSCs

The hBMSC-dSCs were assessed for myelinating function in co-culture with purified and semi-dissociated DRG neurons. By day 14 in co-culture when hBMSC-dSCs were observable in alignment with neurite bundles (Figures 3Aa and 3Ab), supplementation of the medium with ascorbic acid induced myelination. Myelin basic protein (MBP)-positive segments were observable along neurite segments, and these were regularly punctuated by MBP-negative nodes (Figures 3Ac and 3Ad). Parallel co-cultures of the DRG neuron network with hBMSCs (Figures 3Ba and 3Bb) or SCLCs (Figures 3Ca and 3Cb) did not show any

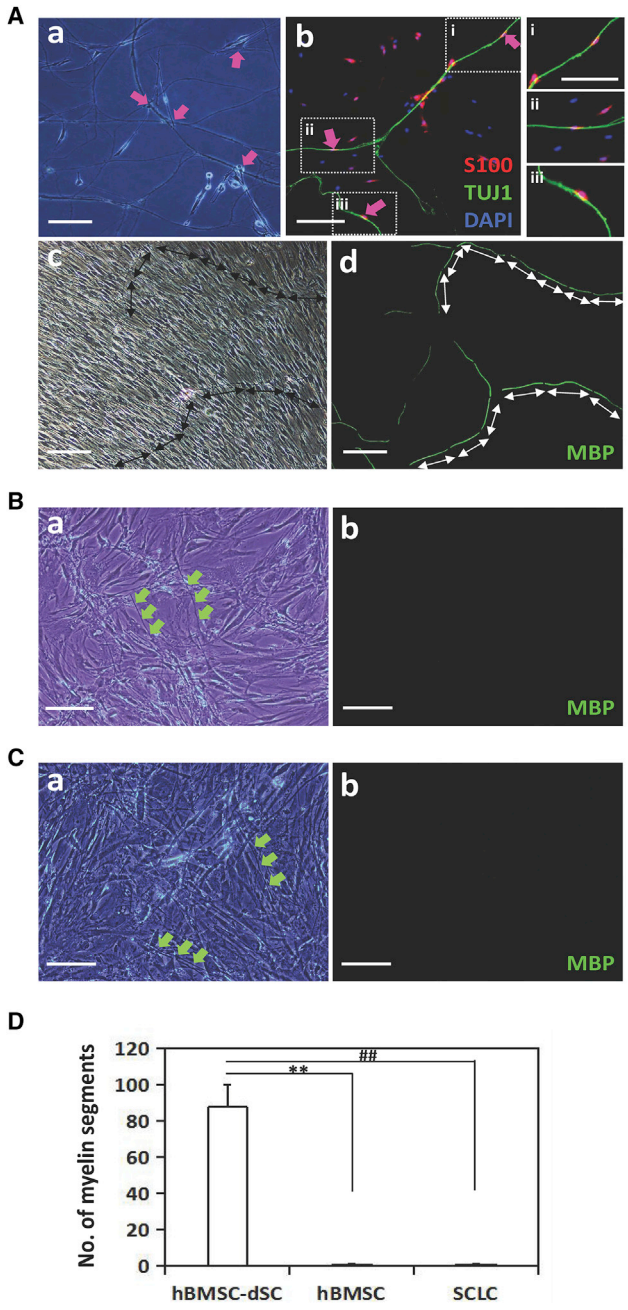

Figure 3. *In Vitro* Myelination of the DRG Neuritic Network by hBMSC-dSCs

(A) Phase-contrast image showing hBMSC-dSCs (arrows) associated with neurons as early as 48 hr in co-culture with the neuritic network of purified DRG neurons in neuron maintenance medium (a). Immunofluorescence for S100 and TUJ1 in a parallel culture showing hBMSC-dSC (arrows) abutting on the neurites (b; right panels, zoom-in views of the boxed areas i–iii). Following 14 days of myelination induction, myelin-like segments (double-headed arrows) were formed by hBMSC-dSCs along the neuritic networks as shown by phase contrast (c) and immunofluorescence for MBP (d). Scale bar, 100 μm.

(B) hBMSCs in parallel co-culture with DRG neurons (arrows) showed a fibroblast-like morphology (a) and failed to form MBP-positive segments along neurites (b). Scale bar, 100 μm.

(C) SCLCs in parallel co-culture with the neuritic network of DRG neurons (arrows) reverted to the myofibroblast phenotype (a) and failed to form MBP-positive segments along neurites (b). Scale bar, 100 μm.

(D) Histogram showing myelinated segment counts in ten fields for hBMSC-dSC versus hardly any for hBMSC (**$p < 0.01$) or SCLCs (##$p < 0.01$). n = 5 independent experiments.

MBP-positive segments. A representative field of view indicated 87.6 ± 12.3 myelinated segments (n = 5, Figure 3D) averaging 102.21 ± 19.73 μm per segment. Having demonstrated myelinating capability of the hBMSC-dSCs *in vitro*, we pursued evidence of such function of hBMSC-dSCs *in vivo*.

hBMSC-dSCs as Source of Neurotrophic Factors

Preliminary to neurite growth studies, hBMSC-dSCs in 24-hr co-culture with Neuro2A cells were assessed for neurotrophic factors produced into the medium. Compared with co-cultures of hBMSCs or SCLCs with Neuro2A cells, those of hBMSC-dSCs indicated significantly higher levels of brain-derived neurotrophic factor (BDNF) (143.2 ± 6.8 versus 51.2 ± 4.4 or 60.5 ± 4.5 pg/mL), vascular endothelial growth factor (VEGF) (4273 ± 280 versus 410 ± 21 or 453 ± 26 pg/mL), hepatocyte growth factor (HGF) (439.5 ± 40.4 versus 62.1 ± 12.4 or 78.0 ± 13.3 pg/mL), and nerve growth factor (NGF) (163.1 ± 12.4 versus 23.1 ± 3.4 or 31.2 ± 4.2 pg/mL). For reference, basal levels ranged from 5 to 20 pg/mL in mono-cultures of Neuro2A cells (Figure 4A). Concentrations were significantly lowered following treatment of the cultures with neutralizing antibodies against the respective neurotrophic factors (Figure 4A). The levels of neurotrophic factors observable in day-1 cultures persisted into day 2 (Figure 4B) when Neuro2A cells were assessed for neurite growth patterns.

Neurotrophic Effects of hBMSC-dSCs

Neuro2A cells in co-culture with hBMSC-dSCs for 48 hr (Figure 5Ad) showed increases in the number and length of neurites when compared with parallel mono-cultures of Neuro2A cells (Figure 5Aa) and co-cultures with hBMSCs (Figure 5Ab) or SCLCs (Figures 5Ac, 5Ba, 5Bb, and 5Bc). The significantly higher percentage of neurite-bearing Neuro2A cells in co-cultures with hBMSC-dSCs versus parallel mono-cultures of Neuro2A cells and co-cultures with hBMSCs or SCLCs (Figure 5B) further suggest enhanced survival. Treating the cultures with neutralizing antibodies against BDNF, VEGF, HGF, NGF, singly or in combination (Figure 5Ae), resulted in significant declines in the percentage of neurite-bearing cells, the length of

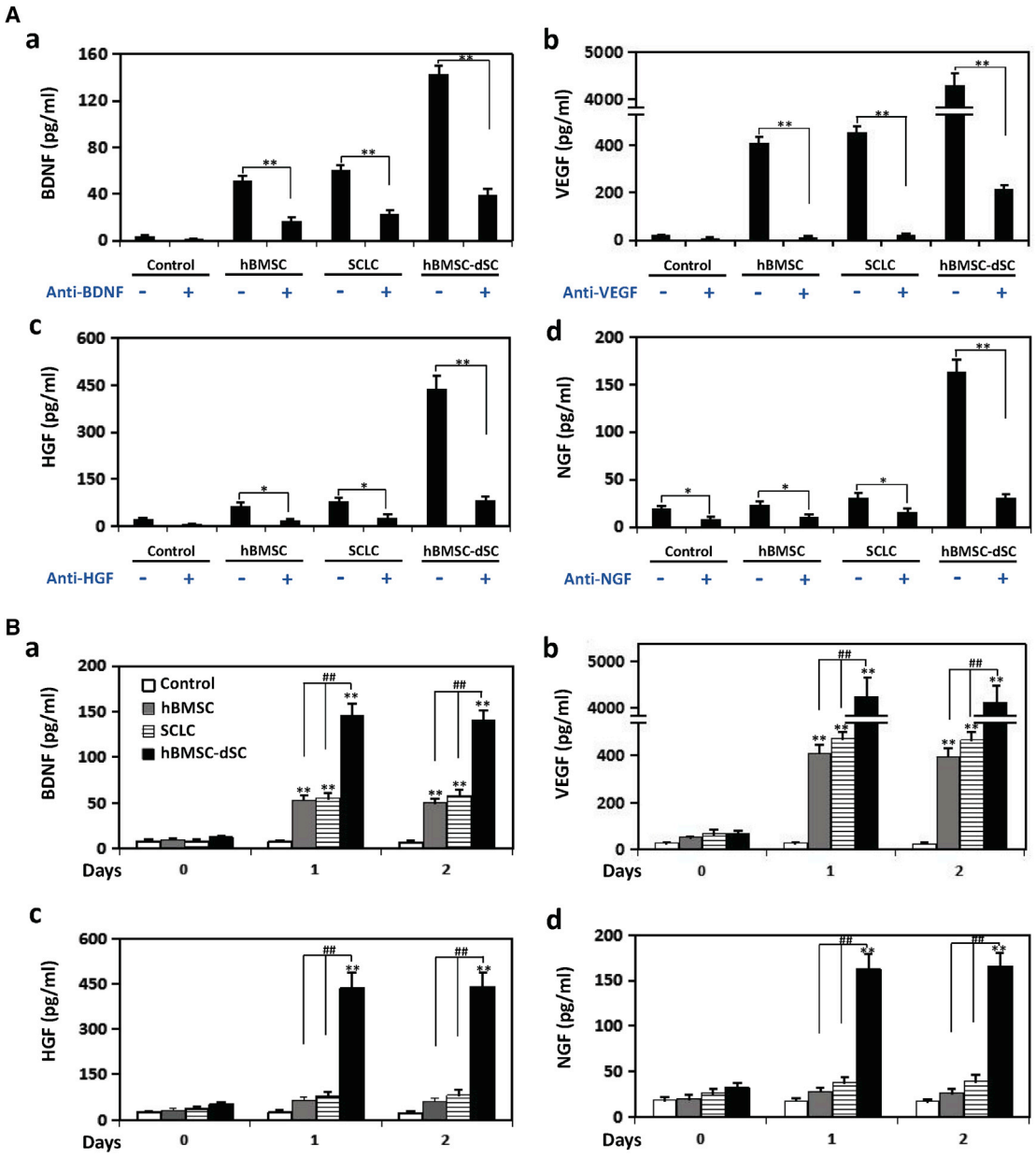

Figure 4. Neurotrophic Factors Secreted by hBMSC-dSCs

(A) Analysis for BDNF (a), VEGF (b), HGF (c), and NGF (d) in medium conditioned by Neuro2A cells (control) versus those in 24-hr co-culture of Neuro2A with hBMSCs, SCLCs, or hBMSC-dSCs. Co-cultures were treated with (+) or without (−) a neutralizing antibody against the indicated factor. The levels of BDNF, VEGF, HGF, and NGF in conditioned media from control, hBMSCs, SCLCs, and hBMSC-dSCs were compared those following antibody treatment. *$p < 0.05$, **$p < 0.01$. n = 5 independent experiments.

(B) Analysis for BDNF (a), VEGF (b), HGF (c), and NGF (d) in medium conditioned by Neuro2A cells (control) versus media conditioned by co-culture of Neuro2A with hBMSCs, SCLCs or hBMSC-dSCs on day 0, 1, or 2. **$p < 0.01$, day 1 or 2 versus day 0; ##$p < 0.01$, hBMSC-dSCs versus hBMSCs or SCLCs. n = 5 independent experiments.

the longest neurite, and the total neurite length per cell, approaching those observed in co-cultures with hBMSCs or SCLCs (Figure 5B). Neuro2A cells thus responded to neurotrophic factors that were produced into the medium of co-cultures with hBMSC-dSCs.

Molecular Phenotype of hBMSC-dSCs

We then used microarrays to compare the gene expression profiles of hBMSCs, SCLCs, hBMSC-dSCs, and adult human SCs (hSCs, ATCC). Hierarchical clustering showed highly similar gene expression profiles of hBMSC-dSCs and hSCs

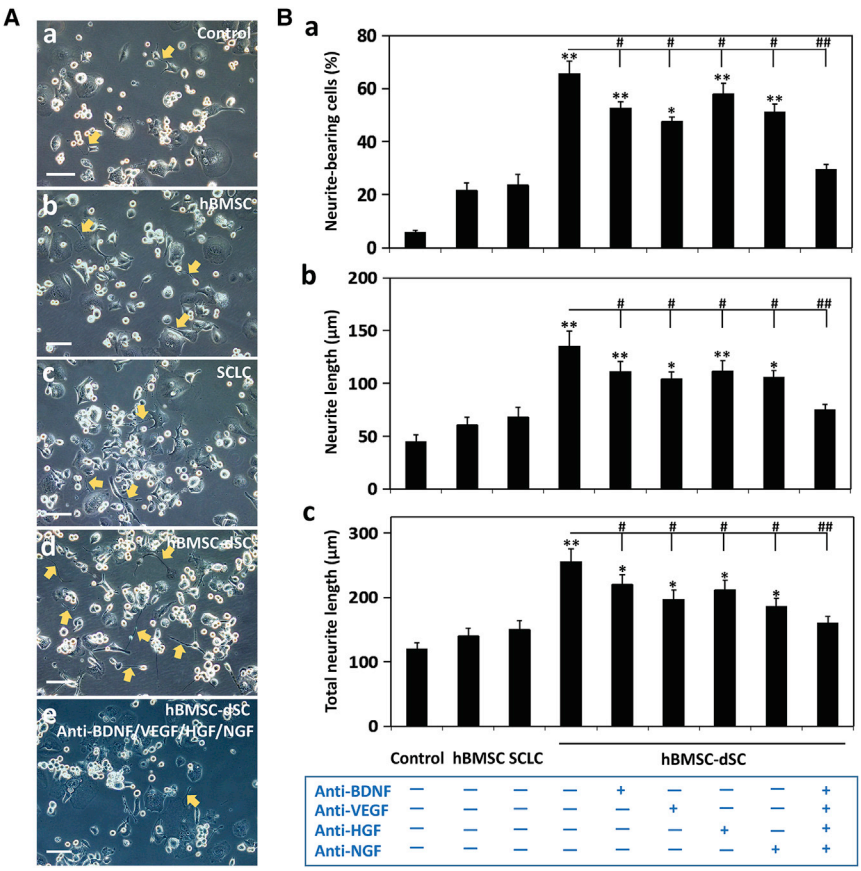

Figure 5. Neurite Outgrowth Mediated by hBMSC-dSCs

(A) Representative images showing phase-contrast views of Neuro2A cells (arrowheads) maintained in neat medium (a, control) versus those in test co-culture for 48 hr with hBMSCs (b), SCLCs (c), hBMSC-dSCs (d), or hBMSC-dSCs with blocking antibodies against BDNF, VEGF, HGF, and NGF supplemented into the culture medium (e). Scale bars, 50 μm.

(B) Histograms showing the percentage of cells bearing at least one neurite ≥ the cell-body diameter (a), length of the longest neurite per cell (b), and total neurite length per cell (c) of Neuro2A cells maintained in neat medium (control) or in test co-culture with hBMSCs, SCLCs, hBMSC-dSCs, or hBMSC-dSCs with blocking antibodies against BDNF, VEGF, HGF, and/or NGF. *p < 0.05, **p < 0.01, hBMSC-dSC with or without blocking antibodies versus hBMSC. #p < 0.05, ##p < 0.01, hBMSC-dSC with blocking antibodies versus hBMSC-dSC without blocking antibodies. n = 5 independent experiments.

as distinct from those of hBMSCs and SCLCs (Figure 6A). This complements the properties of myelination and neurotrophic factor production as evidence that the hBMSC-dSCs were functionally viable. To further investigate the differentiation status of the hBMSC-dSCs, Venn diagrams depicting the distribution of genes upregulated versus those downregulated in SCLCs, hBMSC-dSCs, and the hSCs, in comparison with those in hBMSCs, are shown in Figure 6B. Only 357 genes (166 upregulated and 191 downregulated) were significantly different between hBMSC-dSCs and hSCs; 1,440 genes (692 upregulated and 748 downregulated) were in common. In contrast, between SCLCs and hSCs, up to 1,693 genes (806 upregulated and 887 downregulated) were significantly different, and only 36 genes (16 upregulated and 20 downregulated) were in common (Figure 6B). Further pairwise comparisons revealed the similar expression profiles between hBMSC-dSCs and hSCs, whereas distinct gene expression profiles of hBMSC-dSCs versus hBMSCs, hBMSC-dSCs versus SCLCs, and SCLCs versus hSCs were evident (Figure 6C). A heatmap that targets expression of 64 genes identifiable with the different stages of Schwann cell differentiation (Jessen and Mirsky, 2005; Krause et al., 2014) again showed highly similar profiles of hBMSC-dSCs and hSCs, distinct from those of hBMSCs and SCLCs (Figure 6D). To verify the data obtained via microarray analysis, quantitative real-time PCR (qRT-PCR) was performed on nine differentially expressed genes (Figure 6E). These include markers for neural crest stem cells (AP2), Schwann cell differentiation marker (NOTCH1), Schwann cell precursors (CDH19, SOX2), immature SCs (SOX10, GFAP), non-myelinating SCs (S100), and myelinating SCs (MBP, RPLP0). The qRT-PCR results reinforced the microarray data, indicating that the hBMSC-dSCs are highly similar to hSCs in marker mRNA profile.

Myelination of Regrowing Axons by hBMSC-dSCs *In Vivo*

To demonstrate the capacity of hBMSC-dSCs for myelination *in vivo*, a nerve guide seeded with the cells was used to bridge a critical gap in a rat model of sciatic nerve injury in which host axons regrowing up to the mid-graft region were myelinated by the seeded SCs and progeny (Ao et al., 2011). By 8 weeks post graft, longitudinal sections made in the mid-graft region indicated regrowing fibers, uniaxially aligned, immunopositive for rat TUJ1 (Figure 7A), and in alternation with layers/sheaths immunopositive for human MBP (Figures 7B and 7C). In this mid-graft region, the rows of Hoechst-stained nuclei detectable along

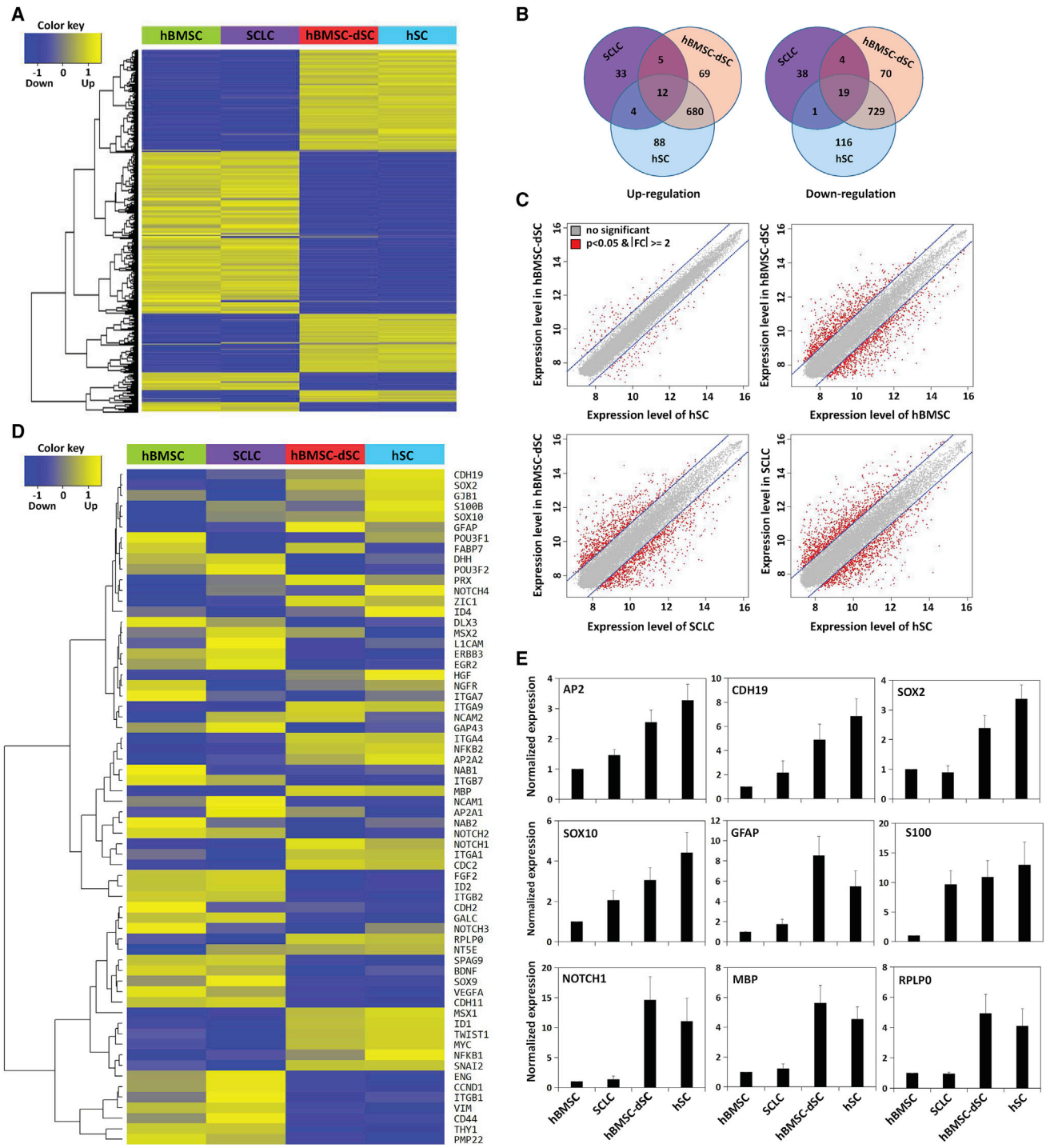

Figure 6. hBMSC-dSCs Are Highly Similar to hSCs

(A) Hierarchical clustering of differentially expressed, overlapped genes illustrated in a heatmap. Blue and yellow indicate the highest and lowest relative levels of expression, as defined by the color key.

(B) Venn diagrams depicting the numbers of genes that are downregulated (left) and upregulated (right) in SCLCs, hBMSC-dSCs, and hSCs, in comparison with hBMSCs.

(C) Pairwise comparisons of expression profile between indicated cells. Blue dashed lines correspond to a 2-fold change. The differentially expressed genes (red) are those that are 2-fold significantly different ($p < 0.05$).

(legend continued on next page)

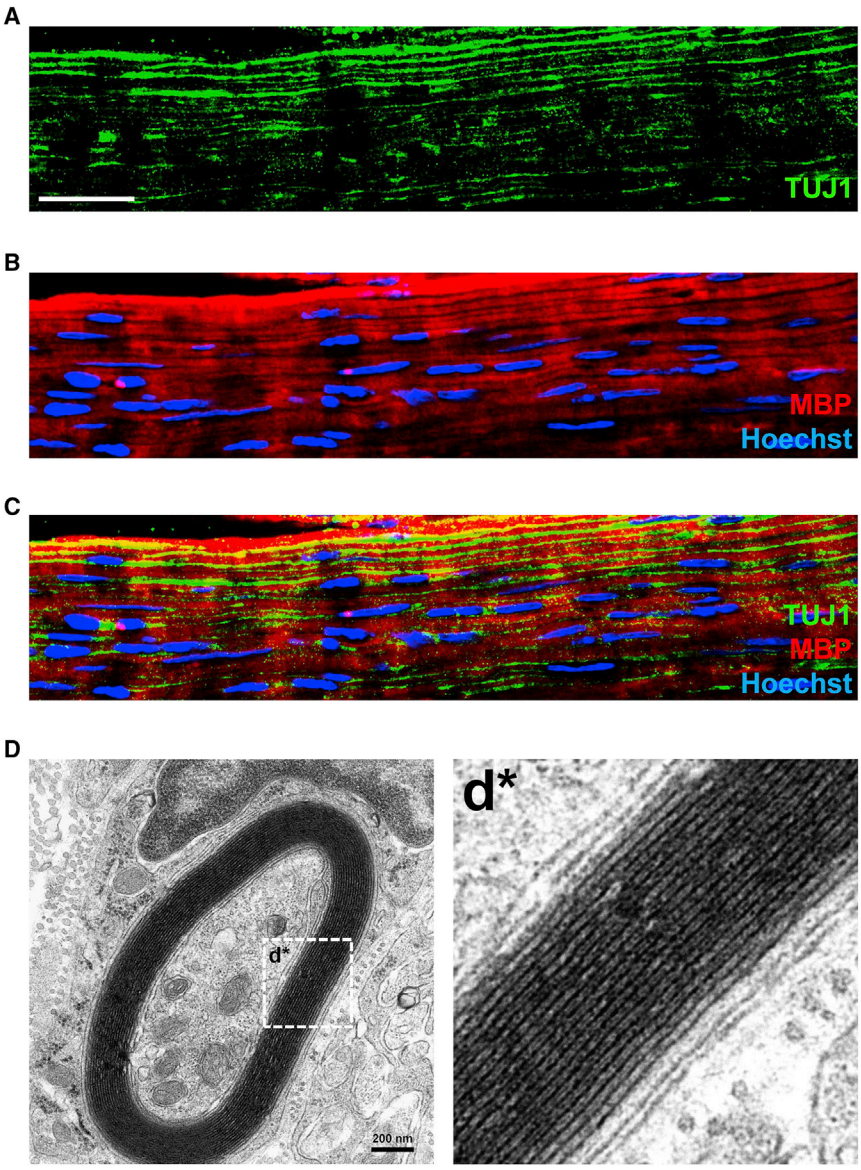

Figure 7. hBMSC-dSCs Myelinated Host Axons by Being Seeded into a Nerve Guide that Bridged a Critical Gap in a Rat Model of Sciatic Nerve Injury

Longitudinal sections made in the mid-region of the sciatic nerve guide reveal the following.

(A) Uni-axially aligned fibers immunopositive for rat TUJ1, representative of regrowing fibers.

(B) Rows of Hoechst-stained nuclei between longitudinal layers immunopositive for human MBP.

(C) Myelin-ensheathed axons and rows of peripherally located nuclei reminiscent of those of Schwann cells in the merged images of (A) and (B).

(D) The myelin structure was illustrated in the TEM image of the transverse section (enlarged in d*). Scale bars, 50 μm for (A)–(C) and 200 nm for (D).

the layers of myelin were reminiscent of the unique geometry of SCs in Büngner regeneration tracks. A representative transmission electron microscopy (TEM) image of a transverse section in the mid-graft region further indicated myelinating SCs at the stage of forming compact myelin (Figures 7D and 7Dd*). Taken together, the results provide *in vivo* evidence of functionally viable hBMSC-dSC subpopulations, some in the repair phenotype guiding axonal regrowth and others adopting the myelinating phenotype.

DISCUSSION

Here, we aimed to derive fate-committed SCs from hBMSCs such that sufficient numbers can be tapped on demand for transplantation to improve the prospects of post-traumatic regrowth and re-myelination of axons and recovery of function. With use of stage-specific culture conditions, we achieved the goal of generating abundant hBMSC-dSCs that show morphological and molecular phenotypes

(D) Heatmap of the microarray data for 64 genes associated with Schwann cell differentiation. Blue and yellow indicate the highest and lowest relative levels of expression, as defined by the color key.

(E) qPCR validation of microarray data. GAPDH served as endogenous standards, and data were normalized against an hBMSC sample.

characteristic of SCs in culture. The hBMSC-dSCs supported neurite growth via secretion of neurotrophic factors and formed PNS-type myelin segments along neurites in *in vitro* tests of function. The purified preparation of hBMSC-dSCs can be kept in storage for at least 3 months in liquid nitrogen and tapped for use in transplantation studies.

Differentiation of the glial progenitors along the SC lineage was fostered in adherent culture of sphere cells. Supplements of basic fibroblast growth factor (bFGF), platelet-derived growth factor (PDGF), β-heregulin, and forskolin were as reported (Dezawa et al., 2001; Keilhoff et al., 2006; Shea et al., 2010). Cells of bi-/tri-polar morphology and expressing markers S100 and p75NTR resulted. These early SCLCs were sustainable as long as the cocktail of extrinsic factors was supplied to the culture. Similarly, Schwann-like cells derived from human adipose-derived mesenchymal stem cells underwent rapid reversion to stem cell-like characteristics following withdrawal of the GIFs (Faroni et al., 2016). Stable *ex vivo* differentiation to maturity must be achieved before the derived SCLCs can be considered safe for therapeutic applications.

SCs are developmentally derived from neural crest cells that coalesce in DRGs following delamination from the neural tube and migration along ventromedial routes (Butler and Bronner, 2015; Schwarz et al., 2009). It is yet unclear how in the course of migration, neural crest cells acquire competence and commitment to the sensory fate. Within the DRGs, specification of peripheral glia is apparently dependent on their association with cells that are committed to neurogenesis (Keilhoff et al., 2006; Marmigere and Ernfors, 2007; Woodhoo et al., 2009). We reasoned that if neural crest cells miss the DRGs and instead enter the developing vasculature, they can end up as residents of the bone marrow and miss out the DRG neuronal signals. We therefore sourced DRG neurons to provide BMSC-derived SCLCs with the necessary signals for SC specification/commitment. DRG neurons of E14/15 rats were readily harvested and purified for use in co-cultures with the hBMSC-SCLCs. The SCLCs progressively acquired the SC phenotype during co-culture and remained stably committed even in subcultures in which extrinsic factors were withdrawn. Neurons were no longer detectable after passage. The DRG neurons were possibly triggered to re-enter the cell cycle but failed to enter the M phase of the cell cycle, thus ending in cell-cycle-related neuronal death (Herrup and Yang, 2007; Zhang et al., 2010). Naive SCLCs that had not been in co-culture with embryonic rat DRG neurons lost the SC phenotype. We conclude that contact-mediating signaling via the incipient sensory neurons is key to directing BMSC-derived SCLCs to SC specification and commitment.

The commitment to SCs is further demonstrated *in vitro* with respect to myelinating and neurotrophic functions. Myelination as a definitive function of mature SCs and MBP, and required for myelin compaction, is used as a marker (Woodhoo et al., 2009; Cai et al., 2017). Our results showed PNS-type MBP-positive segments among the progeny of hBMSC-dSCs in co-culture with the neurite network of purified DRG neurons. The indirect co-culture model of hBMSC-dSCs and Neuro2A cells provided evidence that the neurite growth-promoting response was attributable to BDNF, VEGF, HGF, and NGF produced by hBMSC-dSC. Indeed, BDNF, VEGF, HGF, and NGF produced by SCs after injury are relevant to neuronal survival and axon regrowth following injury (Cai et al., 2011; Taveggia et al., 2010). In addition, the high correlation in gene expression profiles of our hBMSC-dSCs with human SCs in contrast to that of hBMSCs or SCLCs provides confidence that our hBMSC-dSCs are of the human lineage. Within the microenvironment of a nerve guide bridging across a critical gap in the sciatic nerve of a rat model, the hBMSC-dSCs demonstrated capacities for adopting both the repair phenotype for guiding axonal regrowth and the myelinating phenotype with expression of human MBP and formation of compact myelin.

Taken together, this study demonstrates that the human bone marrow harbors neuro-ectodermal progenitors that can be enriched, expanded, and directed to differentiate into functionally mature, fate-committed SCs. The results hold promise for further development into an autologous cell source for implantation as a treatment strategy for nerve injuries or peripheral neuropathies.

EXPERIMENTAL PROCEDURES

Culture of hBMSCs

Human bone marrow was obtained from consenting normal donors 20–30 years of age by puncturing the posterior superior iliac spine under sterile conditions (Lee et al., 2009) with informed consent (Supplemental Experimental Procedures) as approved by the Institutional Review Board, The University of Hong Kong. Samples from six individuals were processed independently.

Induction of Neurospheres from hBMSCs

hBMSCs at passage 4 were seeded at 100,000 cells/mL in serum-free sphere-forming medium consisting of 1:1 (v/v) DMEM/F12 and Neurobasal medium (Invitrogen) supplemented with bFGF (40 ng/mL; Peprotech), epidermal growth factor (20 ng/mL; Peprotech), and B27 (2%, v/v, Invitrogen) into ultra-low-attachment poly(2-hydroxyethyl methacrylate)-coated culture plates (Corning). This non-adherent fraction was maintained for another 3 weeks. The spheres that formed were tested for nestin and GFAP immunoreactivities as neuroprogenitor markers. The sphere formation rate was assessed (Supplemental Experimental Procedures).

Differentiation of Neurosphere Cells into SCLCs

The neurospheres at passage 2 were seeded at 8–10 spheres/cm^2 onto poly-L-lysine/laminin-coated culture dishes. Cultures were

maintained in glutamine-free α-MEM (Sigma) containing 10% fetal bovine serum (FBS) and such GIFs as forskolin (FSK) (5 μM), platelet-derived growth factor (PDGF)-AA (5 ng/mL), bFGF (10 ng/mL), and β-heregulin (HRG) (200 ng/mL) for 2 weeks. Cells immunoreactive for S100 and p75NTR at this stage were referred to as SCLCs. These SCLCs were further cultured in basal medium (DMEM/F12 with 10% FBS) but without the GIFs to test for sustainability of the SC phenotype.

Co-culture of SCLCs with Rat DRG Neurons

Rat DRG neurons were purified and maintained in culture (Shea et al., 2010) (Supplemental Experimental Procedures). SCLCs were seeded onto the DRG neuron culture at 3,000 cells/cm and maintained as co-culture for 2 weeks in glutamine-free α-MEM and Neurobasal medium (1:1, v/v) supplemented with FSK (2.5 μM), PDGF (2.5 ng/mL), bFGF (5 ng/mL), β-HRG (100 ng/mL), NGF (5 ng/mL), B27 (1% v/v), and FBS (5%). Following trypsinization and subculture in basal medium without the GIFs for at least 1 week, neurons did not survive, whereas the surviving cells were all immunopositive for SC markers; these cells were termed hBMSC-dSCs. Neuron cultures that were not seeded with SCLCs were maintained in parallel under the same conditions to exclude the possible contamination of co-cultures with DRG-SCs. Control co-cultures were performed in which a 5-mm-wide hydrophobic barrier prevented direct contact between purified DRG neurons and SCLCs seeded to the left and right of barrier, respectively (Shea et al., 2010).

In Vitro Myelination

Myelination assay (Shea et al., 2010) was performed with hBMSC-dSCs (80,000 cells) seeded onto DRG neuron cultures maintained in neuron maintenance medium supplemented with 10% FBS. Myelination was triggered with ascorbic acid (50 μg/mL, Sigma) added to the medium. Two weeks later, cultures were assessed for MBP immunoreactivity along neurite segments. MBP-positive segments were counted in ten randomly selected fields (magnification, 200×). Co-culture with hBMSCs or SCLCs was set as the negative controls.

Immunofluorescence

Cells were incubated (16 hr, 4°C) with one of the primary antibodies against CD 73 (mouse monoclonal, Abcam, cat. no. ab54217, 1:500), CD 90 (mouse monoclonal, Abcam, cat. no. ab181469, 1:200), CD105 (mouse monoclonal, Abcam, cat. no. ab2529, 1:200), nestin (mouse monoclonal, Abcam, cat. no. ab22035, 1:200), GFAP (mouse monoclonal, Abcam, cat. no. ab49874, 1:1,000), S100 (rabbit monoclonal, Abcam, cat. no. ab52642, 1:100), p75NTR (rabbit polyclonal, Abcam, cat. no. ab8874, 1:500), TUJ1 (rabbit polyclonal, Biolegend, cat. no. 802001, 1:1,000) and MBP (rabbit polyclonal, Abcam, cat. no. ab124493, 1:100). Cells were incubated (2 hr, 24°C) with the appropriate secondary antibodies which included Alexa 488-conjugated goat anti-mouse IgG (polyclonal, Abcam, cat. no. ab150113, 1:500), Alexa 488-conjugated donkey anti-rabbit IgG (polyclonal, Abcam, cat. no. ab150073, 1:500), Alexa 647-conjugated donkey anti-mouse IgG (polyclonal, Abcam, cat. no. ab150107, 1:500), and Alexa 647-conjugated goat anti-rabbit IgG (polyclonal, Abcam, cat. no. ab150079, 1:500). Nuclei were counterstained with 4,6-diamidino-2-phenylindole (DAPI; Abcam). Cells were viewed under an Olympus IX71 inverted fluorescence microscope. For cell counting, ten random fields were selected and a minimum of 500 cells were counted in these fields. The number of marker-positive cells was expressed as a percentage of the total number of cells counted.

Quantitative Real-Time Quantitative PCR

Cells were lysed with Trizol (Invitrogen). Total RNA was extracted and reverse transcribed using SuperScript II First-Strand Synthesis System (Invitrogen) according to the manufacturer's instructions. qRT-PCR was performed using the 9000HT instrument (Applied Biosystems) and SYBR Premix EX Taq (Takara), following the manufacturer's instructions. Each sample was measured in triplicate. Primer sequences are listed in Table S1.

Western Blot Analysis

Whole-cell lysates were prepared, and protein concentrations were assayed (Pan et al., 2009). Equal amounts of protein were subjected to SDS-PAGE and transferred to polyvinylidene difluoride membrane (Millipore Corp.). Membranes were blocked and then probed (16 hr, 4°C) with one of the antibodies against GFAP (mouse monoclonal, Abcam, cat. no. ab8975, 1:500), S100 (rabbit monoclonal, Abcam, cat. no. ab52642, 1:1,000), p75NTR (rabbit polyclonal, Abcam, cat. no. ab8874, 1:500), or nestin (mouse monoclonal, Abcam, cat. no. ab22035, 1:2,000) and β-actin (rabbit polyclonal, Abcam, cat. no. ab8227, 1:1,000) as internal control. Then the membranes were blotted with an appropriate horseradish-peroxidase-linked secondary antibody. Electrochemiluminescence was performed according to the manufacturer's instructions with the ChemiImager 5500 imaging system (Alpha Innotech Co.).

Neurite Outgrowth Analysis

Neurite outgrowth analysis (Mahay et al., 2008; Park et al., 2010) was performed with Neuro2A cells (1×10^5 cells per well) in MEM containing 10% FBS for 16 hr and then in serum-free Neurobasal medium with or without BDNF-, VEGF-, HGF-, and/or NGF-neutralizing antibody for 8 hr. Twenty-four hours earlier, hBMSCs, SLCLs, or hBMSC-dSCs were seeded at 1×10^5 cells per insert (1.0-μm pore size cell-culture inserts, Falcon; BD Biosciences) and maintained in culture for 48 hr. The inserts were then placed onto six-well plates containing Neuro2A cells and maintained for another 48 hr. Cell-free inserts (control) were incubated with Neuro2A cells under the same conditions. Neurite outgrowth was assessed by the percentage of process-bearing neurons, length of longest neurite, and total neurite length per cell with use of SigmaScan Pro 5 software.

Enzyme-Linked Immunosorbant Assay

The conditioned medium from co-cultures of Neuro2A cells and hBMSCs, SLCLs, or hBMSC-dSCs was collected and analyzed by ELISA using the ChemiKine BDNF, VEGF, HGF, or NGF sandwich ELISA kits (Chemicon, UK) according to the manufacturer's protocol. The absorbance was measured at 450 nm (Multiskan MC plate reader; Labsystems).

Microarrays

Total RNA was amplified and purified using a TargetAmp-Nano Labeling Kit for Illumina Expression BeadChip (EPICENTRE, Madison, USA) to yield biotinylated cRNA according to the

manufacturer's instructions. After purification, the cRNA was quantified using the ND-1000 Spectrophotometer (NanoDrop, Wilmington, USA). cRNA samples were hybridized to each human HT-12 v4.0 Expression Beadchip, according to the manufacturer's instructions (Illumina, Inc., San Diego, USA). Detection of array signal was carried out using Amersham fluorolink streptavidin-Cy3 (GE Healthcare Bio-Sciences, Little Chalfont, UK) following the bead array manual. Arrays were scanned with an Illumina bead array Reader confocal scanner according to the manufacturer's instructions. Raw data were extracted using the software Illumina GenomeStudio v2011.1 (Gene Expression Module v1.9.0). Array probes were transformed by logarithm and normalized by the quantile method. Statistical significance of the expression data was determined using the Independent LPE test and fold change, in which the null hypothesis was that no difference exists among groups. The false discovery rate was controlled by adjusting the p value using the Benjamini-Hochberg algorithm. For a DEG set, hierarchical cluster analysis was performed using complete linkage and Euclidean distance as a measure of similarity. Data analysis and visualization of differentially expressed genes were conducted using R 3.1.2 (www.r-project.org).

Grafting Procedure

Grafting experiments were performed on sciatic nerves of pentobarbital-anesthetized (60 mg/kg, intra-peritoneal) male Sprague-Dawley rats (200–250 g). The rat was kept warm on a thermostat-controlled heating pad (37°C) throughout the surgery. The skin on the posterolateral side of the left thigh was incised to expose the sciatic nerve. A 5-mm segment of the nerve was excised at mid-thigh level. The nerve stumps were bridged with a 16-mm long chitosan conduit (2 mm in inner diameter, 0.3 mm in wall thickness) such that the proximal and distal ends of the cut nerve were telescoped 2 mm into the conduit and then secured with polydioxanone sutures (PDS) to the wall of the conduit. The 12-mm interstump gap was pre-filled with (1) hBMSC-dSCs (1.5×10^5 cells in 20 μL DMEM) mixed 1:1 (v/v) with Matrigel (BD) (test) versus (2) 1:1 (v/v) with Matrigel in DMEM (control). The wound was closed in two layers with 6-0 nylon sutures. The immunosuppressant cyclosporin A (Sigma) was administered to the animals (10 mg/kg/day, subcutaneously). The animals were returned to the cages with food and water *ad libitum* for 8 weeks before they were killed. All surgical procedures were performed in strict accordance with the Guide for the Care and Use of Laboratory Animal (National Research Council, USA) and approved by the Committee on Use of Live Animals for Teaching and Research, The University of Hong Kong.

Sample Preparation, Immunohistochemistry, and TEM

The experimental animals were killed with pentobarbital overdose and then perfused with 4% paraformaldehyde. The regenerated tissue cable was dissected out and post-fixed in 4% paraformaldehyde for 2 hr before incubation in 30% sucrose overnight. Longitudinal cryosections (100 μm) were prepared. The sections were permeabilized and blocked with 0.3% Triton X-100 and 3% BSA (1 hr, 20°C) and then incubated with primary antibodies (rabbit anti-rat TUJ1, polyclonal, Biolegend, cat. no. 802001, 1:500; mouse anti-human MBP, monoclonal, Abcam, cat. no. ab11223, 1:500; overnight, 4°C) followed with the relevant secondary antibodies (1 hr, 20°C). Cell nuclei were counterstained with Hoechst 33258. For negative control, isotype antibodies (rabbit IgG and mouse IgG, Invitrogen) were used in lieu of the antigen-specific antibodies (Figure S4). The stained sections were rinsed and mounted with mounting medium (ibidi) for viewing and image capture under confocal microscopy (Zeiss LSM780). For TEM, paraformaldehyde-fixed samples were further treated with 1% osmium tetroxide and 1% uranyl acetate and then embedded in Epon resin. Sections of 75–90 nm thickness were picked up on formvar/carbon-coated 75-mesh Cu grids, and stained for 20 s in 1:1 super-saturated uranyl acetate in acetone followed by 0.2% lead citrate. Images were viewed and captured under a Philips CM100 transmission electron microscope.

Statistical Analysis

All experiments were repeated at least three times unless otherwise indicated. Data are presented as means ± SD. Statistical analysis involved use of the Student t test. Statistical significance was accepted at $p < 0.05$.

ACCESSION NUMBERS

Microarray data in this article have been deposited in the GEO under accession number GEO: GSE102049.

SUPPLEMENTAL INFORMATION

Supplemental Information includes Supplemental Experimental Procedures, four figures, and one table and can be found with this article online at http://dx.doi.org/10.1016/j.stemcr.2017.08.004.

AUTHOR CONTRIBUTIONS

S.C., conception and design, experimentation, data analysis and interpretation, manuscript writing, and final approval of the manuscript; Y.-P.T., conception and experimentation; K.-W.T., animal experiments; G.K-H.S., conception and animal experiments; R.S-K.C., collection of bone marrow for BMSC isolation and culture; Q.A., preparation of the chitosan conduit for grafting experiments; D.K-Y.S. and Y.-S.C., conception and design, data analysis and interpretation, manuscript writing, financial support, and final approval of the manuscript.

ACKNOWLEDGMENTS

This study was supported in part by the National Natural Science Foundation/Research Grants Council Joint Research Scheme (N_HKU741/11), the National Natural Science Foundation of China (nos. 81272080, 81000011), the SK Yee Medical Research Fund, and the Strategic Research Theme on Neuroscience (The University of Hong Kong).

Received: March 15, 2016
Revised: August 11, 2017
Accepted: August 11, 2017
Published: September 7, 2017

REFERENCES

Ao, Q., Fung, C.K., Tsui, A.Y., Cai, S., Zuo, H.C., Chan, Y.S., and Shum, D.K. (2011). The regeneration of transected sciatic nerves of adult rats using chitosan nerve conduits seeded with bone marrow stromal cell-derived Schwann cells. Biomaterials *32*, 787–796.

Bachelin, C., Lachapelle, F., Girard, C., Moissonnier, P., Serguera-Lagache, C., Mallet, J., Fontaine, D., Chojnowski, A., Le Guern, E., Nait-Oumesmar, B., et al. (2005). Efficient myelin repair in the macaque spinal cord by autologous grafts of Schwann cells. Brain *128*, 540–549.

Brosius Lutz, A., and Barres, B.A. (2014). Contrasting the glial response to axon injury in the central and peripheral nervous systems. Dev. Cell *28*, 7–17.

Brushart, T.M., Aspalter, M., Griffin, J.W., Redett, R., Hameed, H., Zhou, C., Wright, M., Vyas, A., and Hoke, A. (2013). Schwann cell phenotype is regulated by axon modality and central-peripheral location, and persists in vitro. Exp. Neurol. *247*, 272–281.

Butler, S.J., and Bronner, M.E. (2015). From classical to current: analyzing peripheral nervous system and spinal cord lineage and fate. Dev. Biol. *398*, 135–146.

Caddick, J., Kingham, P.J., Gardiner, N.J., Wiberg, M., and Terenghi, G. (2006). Phenotypic and functional characteristics of mesenchymal stem cells differentiated along a Schwann cell lineage. Glia *54*, 840–849.

Cai, S., Shea, G.K., Tsui, A.Y., Chan, Y.S., and Shum, D.K. (2011). Derivation of clinically applicable Schwann cells from bone marrow stromal cells for neural repair and regeneration. CNS Neurol. Disord. Drug Targets *10*, 500–508.

Cai, S., Han, L., Ao, Q., Chan, Y.S., and Shum, D.K. (2017). Human induced pluripotent cell-derived sensory neurons for fate commitment of bone marrow-derived Schwann cells: implications for remyelination therapy. Stem Cells Transl. Med. *6*, 369–381.

Chen, Z.L., Yu, W.M., and Strickland, S. (2007). Peripheral regeneration. Annu. Rev. Neurosci. *30*, 209–233.

Dezawa, M., Takahashi, I., Esaki, M., Takano, M., and Sawada, H. (2001). Sciatic nerve regeneration in rats induced by transplantation of in vitro differentiated bone-marrow stromal cells. Eur. J. Neurosci. *14*, 1771–1776.

Faroni, A., Smith, R.J., Lu, L., and Reid, A.J. (2016). Human Schwann-like cells derived from adipose-derived mesenchymal stem cells rapidly de-differentiate in the absence of stimulating medium. Eur. J. Neurosci. *43*, 417–430.

Gomez-Sanchez, J.A., Carty, L., Iruarrizaga-Lejarreta, M., Palomo-Irigoyen, M., Varela-Rey, M., Griffith, M., Hantke, J., Macias-Camara, N., Azkargorta, M., Aurrekoetxea, I., et al. (2015). Schwann cell autophagy, myelinophagy, initiates myelin clearance from injured nerves. J. Cell Biol. *210*, 153–168.

Herrup, K., and Yang, Y. (2007). Cell cycle regulation in the postmitotic neuron: oxymoron or new biology? Nat. Rev. Neurosci. *8*, 368–378.

Jessen, K.R., and Mirsky, R. (2005). The origin and development of glial cells in peripheral nerves. Nat. Rev. Neurosci. *6*, 671–682.

Keilhoff, G., Goihl, A., Langnase, K., Fansa, H., and Wolf, G. (2006). Transdifferentiation of mesenchymal stem cells into Schwann cell-like myelinating cells. Eur. J. Cell Biol. *85*, 11–24.

Krause, M.P., Dworski, S., Feinberg, K., Jones, K., Johnston, A.P., Paul, S., Paris, M., Peles, E., Bagli, D., Forrest, C.R., et al. (2014). Direct genesis of functional rodent and human Schwann cells from skin mesenchymal precursors. Stem Cell Reports *3*, 85–100.

Lee, K.A., Shim, W., Paik, M.J., Lee, S.C., Shin, J.Y., Ahn, Y.H., Park, K., Kim, J.H., Choi, S., and Lee, G. (2009). Analysis of changes in the viability and gene expression profiles of human mesenchymal stromal cells over time. Cytotherapy *11*, 688–697.

Mahay, D., Terenghi, G., and Shawcross, S.G. (2008). Schwann cell mediated trophic effects by differentiated mesenchymal stem cells. Exp. Cell Res. *314*, 2692–2701.

Marmigere, F., and Ernfors, P. (2007). Specification and connectivity of neuronal subtypes in the sensory lineage. Nat. Rev. Neurosci. *8*, 114–127.

Martini, R., Fischer, S., Lopez-Vales, R., and David, S. (2008). Interactions between Schwann cells and macrophages in injury and inherited demyelinating disease. Glia *56*, 1566–1577.

Pan, Y., Ren, K.H., He, H.W., and Shao, R.G. (2009). Knockdown of Chk1 sensitizes human colon carcinoma HCT116 cells in a p53-dependent manner to lidamycin through abrogation of a G2/M checkpoint and induction of apoptosis. Cancer Biol. Ther. *8*, 1559–1566.

Park, H.W., Lim, M.J., Jung, H., Lee, S.P., Paik, K.S., and Chang, M.S. (2010). Human mesenchymal stem cell-derived Schwann cell-like cells exhibit neurotrophic effects, via distinct growth factor production, in a model of spinal cord injury. Glia *58*, 1118–1132.

Rodriguez, F.J., Verdu, E., Ceballos, D., and Navarro, X. (2000). Nerve guides seeded with autologous Schwann cells improve nerve regeneration. Exp. Neurol. *161*, 571–584.

Rosenberg, A.F., Isaacman-Beck, J., Franzini-Armstrong, C., and Granato, M. (2014). Schwann cells and deleted in colorectal carcinoma direct regenerating motor axons towards their original path. J. Neurosci. *34*, 14668–14681.

Schwarz, Q., Maden, C.H., Vieira, J.M., and Ruhrberg, C. (2009). Neuropilin 1 signaling guides neural crest cells to coordinate pathway choice with cell specification. Proc. Natl. Acad. Sci. USA *106*, 6164–6169.

Shea, G.K., Tsui, A.Y., Chan, Y.S., and Shum, D.K. (2010). Bone marrow-derived Schwann cells achieve fate commitment–a prerequisite for remyelination therapy. Exp. Neurol. *224*, 448–458.

Taveggia, C., Feltri, M.L., and Wrabetz, L. (2010). Signals to promote myelin formation and repair. Nat. Rev. Neurol. *6*, 276–287.

Woodhoo, A., Alonso, M.B., Droggiti, A., Turmaine, M., D'Antonio, M., Parkinson, D.B., Wilton, D.K., Al-Shawi, R., Simons, P., Shen, J., et al. (2009). Notch controls embryonic Schwann cell differentiation, postnatal myelination and adult plasticity. Nat. Neurosci. *12*, 839–847.

Zhang, J., Li, H., Yabut, O., Fitzpatrick, H., D'Arcangelo, G., and Herrup, K. (2010). Cdk5 suppresses the neuronal cell cycle by disrupting the E2F1-DP1 complex. J. Neurosci. *30*, 5219–5228.